

WST-X Series: Wavelet Scattering Transform for Interpretable Speech Deepfake Detection

Xi Xuan, Davide Carbone, Ruchi Pandey, Wenxin Zhang, Tomi H. Kinnunen

Abstract—Designing front-ends for speech deepfake detectors primarily focuses on two categories. Hand-crafted filterbank features are transparent but are limited in capturing high-level semantic details, often resulting in performance gaps compared to self-supervised (SSL) features. SSL features, in turn, lack interpretability and may overlook fine-grained spectral anomalies. We propose the WST-X series, a novel family of feature extractors that combines the best of both worlds via the wavelet scattering transform (WST), integrating wavelets with nonlinearities analogous to deep convolutional networks. We investigate 1D and 2D WSTs to extract acoustic details and higher-order structural anomalies, respectively. Experimental results on the recent and challenging Deepfake-Eval-2024 dataset indicate that WST-X outperforms existing front-ends by a wide margin. Our analysis reveals that a small averaging scale (J), combined with high-frequency and directional resolutions (Q, L), is critical for capturing subtle artifacts. This underscores the value of translation-invariant and deformation-stable features for robust and interpretable speech deepfake detection.

Index Terms—Speech deepfake, Wavelet scattering transform, Scattering coefficients, Audio forensics, Interpretability.

I. INTRODUCTION

Speech deepfake detectors (SDDs) aim to distinguish artificially generated speech from real human speech. SDD systems consist of a front-end (feature extractor) [1–3] followed by a back-end (classifier) [4–6]. The choice of the former is critical as it determines the SDD’s ability to capture subtle acoustic artifacts suitable for deepfake detection. SDD front-ends can be broadly categorized into digital signal processing (DSP) and self-supervised learning (SSL) approaches, each offering distinct advantages.

The former category utilizes time-frequency analysis techniques based on the short-time Fourier transform (STFT) [7], including mel-spectrograms [8] and linear-frequency cepstral coefficients (LFCCs) [7]. These representations are obtained by applying a bank of frequency-localized filters to the STFT magnitude spectra, resulting in a low-dimensional representation. Early studies also used the constant-Q transform, a multiresolution time-frequency method adopted from music signal processing, to extract corresponding cepstral coefficients, CQCCs [9]. Despite transparency, simplicity, and computational efficiency, these features are limited in their lack

Xi Xuan (Corresponding author, xi.xuan@uef.fi), Tomi H. Kinnunen (tomi.kinnunen@uef.fi), and Ruchi Pandey (ruchi@uef.fi), are affiliated with the Computational Speech Group at the University of Eastern Finland.

Davide Carbone (davide.carbone@phys.ens.fr) is affiliated with Laboratoire de Physique de l’Ecole Normale Supérieure, Université PSL, CNRS, Sorbonne Université, Université de Paris, Paris, France.

Wenxin Zhang (zhangwenxin23@mails.ucas.ac.cn) is with the School of Computer Science and Technology at the University of Chinese Academy of Sciences and the Department of Mathematics at the University of Toronto.

of robustness, suboptimal time-frequency analysis properties, and spectral smoothing introduced by the filterbank.

On the other hand, modern SSL models, such as XLSR [10], HuBERT [11], and MMS [12], provide a robust, data-driven alternative to hand-crafted filterbank feature extraction. They are trained on massive amounts of data, leveraging data augmentation and masking techniques to learn representations robust to noisy or missing observations. While SSLs outperform pure DSP front-ends in detection and generalization, they suffer from high computational costs, potential overfitting, and limited explainability. This limitation is a particular concern in audio forensic investigations, where model interpretability is not merely a desirable property but a fundamental requirement; scientific evidence should be transparent, reproducible, and open to scrutiny [13].

To address these shortcomings, our work introduces, for the first time, the *wavelet scattering transform* (WST) [14–16] to SDD. WST serves as a bridge between DSP-based and data-driven front-ends, as it can be interpreted as a mathematical counterpart to convolutional layers in neural networks. *Importantly, WST requires no training data* but is entirely defined through invariance and stability properties concerning signal translation and deformation. Furthermore, the hierarchical structure of the scattering coefficients offers a clear physical interpretation of multiscale processes, making it suitable for analyzing complex natural sounds [17–19].

Marking the first study of its kind, we propose **WST-X**, a novel family of front-ends for speech deepfake detection, providing comprehensive experimental analysis using state-of-the-art back-end [4] on a recent, challenging in-the-wild deepfake detection benchmark [20]. Our study focuses on how to best integrate the complementary strengths of WST- and SSL-based front-ends, exploring both parallel and cascaded integration strategies. These two representations maintain mathematical stability and interpretability, while concurrently capturing both subtle local acoustic artifacts and high-level linguistic or semantic traits. To this end, we address the following research questions (RQs):

RQ1. What are the suitable parameters for the 1D and 2D wavelet scattering transform for speech deepfake detection?

RQ2. What is the relative performance gain of WST-X extractors compared to traditional acoustic features?

RQ3. How can 1D and 2D WST be integrated with SSL features to provide complementary acoustic details? Which fusion strategy achieves better detection performance?

By addressing these questions, our work provides the first evaluation of WST-based representations for speech deepfake detection, laying a foundation for future research in this area.

II. PROPOSED METHOD

In this section, we detail the WST-X Series designed for SDD. We begin by introducing the fundamentals of the wavelet scattering transform theory and its physical parameters, followed by a detailed description of our novel feature extractors.

A. Wavelet Scattering Transform Theory

The wavelet scattering transform (WST) [14, 15] stands as a mathematical operator capable of yielding a stable and invariant representation for a speech signal $x(t)$ through a cascade of wavelet modulus operators, as illustrated in Fig. 1. For discrete signals sampled at f_s , this analysis is performed over a temporal invariance scale $T = 2^J/f_s$ seconds, where 2^J denotes the window size. This cascade is parameterized by a path $p = (\lambda_1, \dots, \lambda_m)$, defined as a tuple of length m built using indices $\lambda_i \in \Lambda^J$ representing an ordered sequence of wavelet scales; the wavelet scattering coefficient $S_J[p]x(t)$ along a path p is defined as the convolution of a propagation operator $U[p]x$ with a scaled Gaussian low-pass filter ϕ_{2^J} :

$$S_J[p]x(t) = (U[p]x * \phi_{2^J})(t) = \int_{-\infty}^{\infty} U[p]x(\tau) \phi_{2^J}(t - \tau) d\tau, \quad (1)$$

where the nonlinear cascade operator is defined as:

$$U[\lambda]x(t) = |(x * \psi_{\lambda})(t)|, \quad U[p]x = U[\lambda_m] \cdots U[\lambda_1]x. \quad (2)$$

Here, $*$ denotes convolution and $\phi_{2^J}(t) = 2^{-J}\phi(t/2^J)$. We define wavelets as $\psi_{\lambda}(t) = \lambda^{-1}\psi(t/\lambda)$, which preserves the L^1 -norm across scale, following Kymatio [21], a popular open-source library for scattering transforms.

To effectively capture the spectral richness of speech signals, we employ scales $\lambda \in \{2^{j/Q}\}_{0 \leq j < JQ}$, where Q is the number of wavelets per octave that determines the log-frequency sampling resolution. These range from dyadic to finer intermediate scales, restricted to remain finer than the averaging scale 2^J . While wavelet transforms [22] provide stability under the action of small diffeomorphisms, the nonlinear operation and the integration over time yield translation invariance [14]. Higher-order cascades recover high-frequency modulation patterns that are lost due to the low-pass averaging of the modulus of lower-order coefficients.

B. Physical Interpretation of WST Parameters

We use the Kymatio library [21] to implement both 1D and 2D WSTs, which form the foundational basis for our WST-X front-ends. The 1D transform operates directly on raw waveforms, whereas the 2D transform processes time-frequency representations, such as spectrograms. The theoretical foundation established above pertains to 1D signals, whereas an extension to higher dimensions (2D WST) can be found in [15]. Complex Morlet wavelets [23] are utilized for the cascaded operations. The 1D WST is characterized by three primary control parameters. First, the averaging scale J ($J \geq 2$) determines the window size 2^J , with smaller J preserving higher-frequency temporal details. Second, the number of wavelets per octave Q ($Q \geq 1$) determines the frequency resolution. Finally, the scattering order $M \in \{1, 2, 3\}$ extracts hierarchical features, including energy envelopes, modulation dynamics, and higher-order interactions.

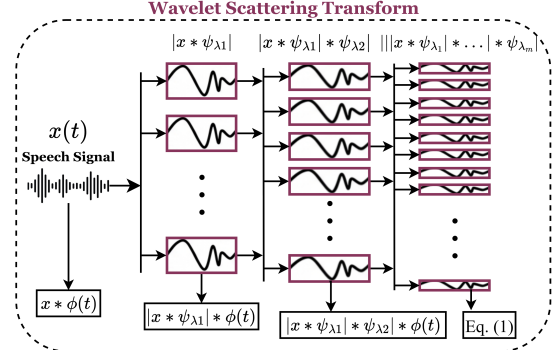


Fig. 1: Hierarchical architecture of the second-order wavelet scattering transform, showing the extraction of zeroth-, first-, and second-order coefficients.

For the 2D WST, we use SSL latent feature maps as input, viewed as two-dimensional images in the (time, feature) plane, analogous to time-frequency representations but with spectral magnitudes replaced by SSL features. The 2D WST is characterized by three hyperparameters. First, the averaging scale J , which defines the maximum spatial scale of the 2D low-pass filter in powers of 2, governs the degree of averaging across both time and frequency axes. Second, the angular resolution L , representing the number of orientations in the 2D wavelet bank to provide directional selectivity, is crucial for capturing spectral structures such as horizontal harmonics, slanted formant transitions, and vertical onsets. Finally, the scattering order M is defined as in the 1D case.

C. WST-X Series Feature Extractor

In principle, WST could be used as a standalone acoustic front-end similar to MFCCs, LFCCs, or CQCCs [7, 9]. However, by capitalizing on the robustness of SSL models such as XLSR [24, 25], we propose the WST-X series front-end, which combines WST and SSL features to bridge the gap between physical signal representations and high-dimensional semantic embeddings. As shown in Fig. 2, the WST-X series comprises two architectural designs: *parallel* (WST-X1) and *cascaded* (WST-X2), detailed as follows.

Prompt Tuning XLSR (PT-XLSR). We adopt XLSR-300M as the foundation model, adhering to the parameter-efficient prompt tuning setup (PT-XLSR) described in [26, 27]. We freeze the XLSR parameters and introduce k learnable prompt tokens $V_i \in \mathbb{R}^{k \times D}$ at each transformer layer $i \in \{1, \dots, 24\}$, where D denotes the hidden dimensionality. The CNN-extracted features $E_0 \in \mathbb{R}^{T \times D}$, where T is the number of time frames, are concatenated with the prompt tokens to guide the encoding process, producing the final representation $E_{24} \in \mathbb{R}^{(k+T) \times D}$ for subsequent integration strategies.

Strategy I: Parallel Integration (WST-X1). WST-X1 is formulated as a parallel dual-branch architecture comprising the 1D WST and PT-XLSR components, both of which operate directly on the raw waveform. To align the feature spaces from both branches, the 1D WST branch extracts scattering coefficients and processes them via global average pooling, linear projection, and temporal expansion. Concurrently, the PT-XLSR branch linearly projects E_{24} from the transformer hidden dimension D to 144. Finally, the outputs from both branches are concatenated channel-wise, resulting in the fused representation $Y_{X1} \in \mathbb{R}^{(k+T) \times 288}$.

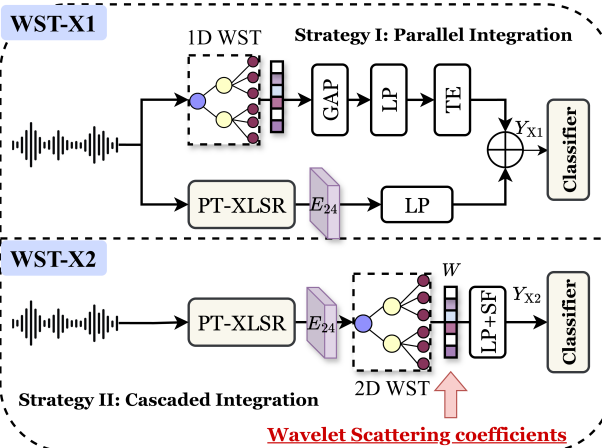


Fig. 2: Overview of the WST-X Series: WST-X1 and WST-X2 feature extractors. The top panel illustrates Strategy I (parallel integration with 1D WST), while the bottom panel shows Strategy II (cascaded integration with 2D WST). GAP (Global Average Pooling); LP (Linear Projection); TE (Temporal Expansion); SF (Spatial Flattening).

Strategy II: Cascaded Integration (WST-X2). WST-X2 uses a cascaded single-pathway architecture. The waveform is first processed by PT-XLSR to extract high-level SSL latent feature maps E_{24} , which are fed into a 2D WST to characterize intra-channel temporal dynamics and inter-channel structural correlations, obtaining a scattering tensor $W \in \mathbb{R}^{C_{\text{path}} \times T' \times D_{\text{scat}}}$. Here, $T' = \lfloor (k + T)/2^J \rfloor$ and $D_{\text{scat}} = \lfloor D/2^J \rfloor$ denote the downsampled temporal and spectral resolutions, respectively. The number of scattering channels C_{path} is determined by concatenating coefficients up to the second order [15], comprising 1 zeroth-order, JL first-order, and $L^2 \binom{J}{2}$ second-order paths. Thus, the total dimension is $C_{\text{path}} = 1 + JL + L^2 J(J-1)/2$. These scattering coefficients capture multi-order spectro-temporal details. Finally, a linear projection reduces D_{scat} to 144, followed by a spatial flatten to reshape the tensor into $Y_{X2} \in \mathbb{R}^{L_{\text{seq}} \times 144}$, where $L_{\text{seq}} = T' \times C_{\text{path}}$.

Classifier. The extracted feature $\mathbf{Y} \in \{Y_{X1}, Y_{X2}\}$ is fed into a recent and robust classifier [4] to produce a probability score \hat{p} , thereby classifying the input speech as real or fake.

III. EXPERIMENTAL SETUP

A. Real-world Dataset Description and Evaluation Metrics

We adopt the recent and challenging Deepfake-Eval-2024 (DE2024) dataset [20] for our experiments, representative of real-world deepfake generation techniques. This multimodal dataset comprises 56.5 hours of real and fake audio content collected from social media platforms and deepfake detection services in 2024, encompassing over 80 web sources and 40 languages. We focus on the audio portion, originally sampled at 44.1 kHz. Following [26], audio samples from the official training and test sets were sliced into non-overlapping 4-second chunks. For a recording of duration T seconds, we extracted $\lfloor T/4 \rfloor$ segments and discarded the remainder, generating a dataset of ~ 50 wav files. Finally, the official training set was split into a train and dev set at a 9:1 ratio, while the official test set remained unchanged.

Our selected performance metrics include minDCF, EER, F1-score, and AUC. While these assess complementary aspects of detection performance, minDCF is our primary metric, providing a scenario-centered assessment of *decision risk* based

TABLE I: Deepfake-Eval-2024 results for WST-X series feature extractor (FE) under different parameter settings, each combined with a shared Mamba-based classifier. Best results are in **bold**. Confidence intervals are in parentheses.

FE	J	Q	M	minDCF \downarrow	EER(%) \downarrow	F1(%) \uparrow	AUC(%) \uparrow	
WST-X1	2	1	2	0.3540 (± 0.0157)	15.19 (± 0.52)	82.14 (± 0.62)	92.13 (± 0.37)	
	2	8	2	0.3682 (± 0.0139)	14.98 (± 0.50)	78.37 (± 0.66)	89.45 (± 0.58)	
	2	10	2	0.3408 (± 0.0161)	14.18 (± 0.63)	81.66 (± 0.58)	92.50 (± 0.40)	
	4	10	2	0.4182 (± 0.0099)	15.04 (± 0.41)	76.85 (± 0.67)	90.35 (± 0.47)	
	6	10	2	0.4172 (± 0.0087)	17.20 (± 0.89)	76.53 (± 0.42)	90.84 (± 0.24)	
	8	10	2	0.4782 (± 0.0122)	16.77 (± 0.41)	79.11 (± 0.63)	89.93 (± 0.34)	
	2	10	3	0.4147 (± 0.0127)	14.93 (± 0.54)	80.78 (± 0.69)	91.23 (± 0.34)	
WST-X2	2	1	2	0.3901 (± 0.0126)	16.37 (± 0.58)	75.40 (± 0.70)	90.82 (± 0.44)	
	FE	J	L	M	minDCF \downarrow	EER% \downarrow	F1% \uparrow	AUC% \uparrow
	2	1	2	2	0.4852 (± 0.0167)	17.00 (± 0.52)	75.19 (± 0.83)	85.98 (± 0.48)
	2	2	2	2	0.3661 (± 0.0123)	14.99 (± 0.58)	75.08 (± 0.64)	91.26 (± 0.35)
	2	4	2	2	0.4180 (± 0.0121)	16.70 (± 0.57)	79.79 (± 0.74)	89.89 (± 0.40)
	2	6	2	2	0.4010 (± 0.0119)	15.60 (± 0.53)	80.30 (± 0.64)	91.14 (± 0.41)
	2	8	2	2	0.3703 (± 0.0142)	14.94 (± 0.52)	79.88 (± 0.60)	90.08 (± 0.37)
WST-X2	2	10	2	2	0.3567 (± 0.0081)	14.84 (± 0.40)	81.83 (± 0.47)	92.43 (± 0.23)
	2	1	3	3	0.4042 (± 0.0111)	15.06 (± 0.38)	80.14 (± 0.57)	89.86 (± 0.39)
	2	2	3	3	0.4186 (± 0.0123)	15.13 (± 0.50)	80.63 (± 0.56)	90.22 (± 0.33)
	2	6	3	3	0.3811 (± 0.0095)	14.96 (± 0.42)	81.09 (± 0.58)	90.16 (± 0.33)
	2	8	3	3	0.3883 (± 0.0164)	15.24 (± 0.74)	79.23 (± 0.78)	91.18 (± 0.46)
	2	10	3	3	0.3743 (± 0.0087)	14.98 (± 0.21)	81.57 (± 0.49)	91.40 (± 0.36)
	3	8	1	3	0.4764 (± 0.0141)	17.24 (± 0.69)	78.71 (± 0.69)	85.60 (± 0.59)
WST-X2	3	8	2	3	0.4284 (± 0.0153)	17.81 (± 0.50)	78.94 (± 0.59)	89.50 (± 0.40)
	3	8	3	3	0.4939 (± 0.0146)	18.21 (± 0.46)	76.48 (± 0.74)	87.22 (± 0.56)

on supplied decision costs and class priors. The normalized detection cost function (DCF) is $\text{DCF}(\tau_{\text{cm}}) = \beta P_{\text{miss}}^{\text{cm}}(\tau_{\text{cm}}) + P_{\text{fa}}^{\text{cm}}(\tau_{\text{cm}})$, where $\beta = (C_{\text{miss}}/C_{\text{fa}}) \cdot (1 - \pi_{\text{spf}})/\pi_{\text{spf}}$. Here, τ_{cm} is the detection threshold, π_{spf} is the assumed prior probability of spoofing attack, and C_{miss} and C_{fa} are the costs of a miss and a false alarm, respectively. We adopt the parameters used in the ASVspoof 5 challenge [28]: $C_{\text{miss}} = 1$, $C_{\text{fa}} = 10$, $\pi_{\text{spf}} = 0.05$, which implies $\beta \approx 1.90$. The DCF is then used to compute the *minimum* normalized DCF, defined as $\text{minDCF} = \min_{\tau_{\text{cm}}} \text{DCF}(\tau_{\text{cm}})$. To ensure statistical reliability, we report two times the standard deviation for all four metrics using 1,000 bootstrap runs [29] on the test dataset.

B. Model Configurations

We evaluate SDD systems by pairing different front-ends with a shared classifier [4]. We use Librosa [30] to downsample the raw audio to 16 kHz and extract the mel, linear, and constant-Q (CQ) filterbank features. To ensure a fair comparison, all features are extracted using a 10 ms hop length. Mel and linear filterbank features employ a 25 ms frame size and a Hanning window, while CQ filterbank uses 9 bins per octave to define the frequency resolution, resulting in feature matrices of shape (80, 399). Both 1D and 2D WST were implemented using Kymatio [21]. To explore suitable control parameters (defined in Sec. II-B), we conducted comparative experiments by selecting J , Q , and M for 1D WST, and J , L , and M for 2D WST. For PT-XLSR, following [31, 32], we adopt XLSR-300M. Concatenating $k = 6$ prompt tokens with the CNNs output E_0 of shape (199, 1024) results in a combined tensor of shape (205, 1024). The classifier comprises 12 Mamba-based blocks [4]. The model is trained for 100 epochs ($lr = 5 \times 10^{-4}$) using binary cross-entropy loss, selecting the checkpoint minimizing dev set EER.

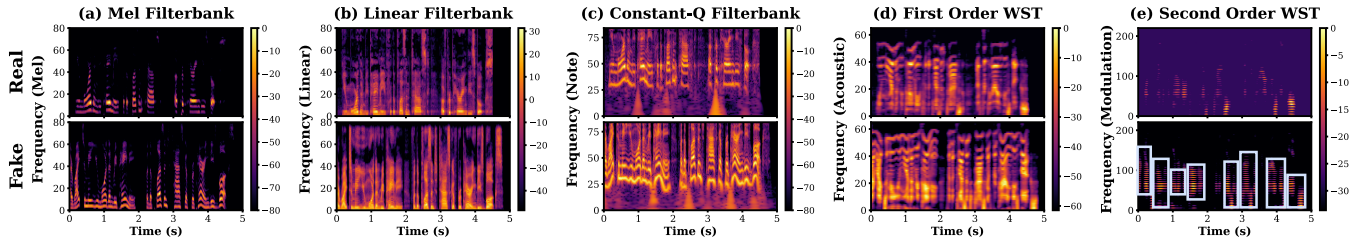


Fig. 3: Representations of a real utterance (top row) and a fake utterance synthesized by Qwen2.5-Omni (bottom row) across different front-ends: (a) Mel, (b) Linear, (c) Constant-Q Filterbank, (d) First-order WST, and (e) Second-order WST. The displayed WST representations correspond to the configuration $(J, Q) = (2, 10)$. Focusing on the bottom row, the correspondence between larger WST scales and lower spectrogram frequencies is visually evident. Notably, the preceding three spectrogram representations appear more coarse-grained than the first- and second-order WST, despite similar overall heatmap patterns. The blue bounding boxes highlight the visually distinctive parts of the fake speech signals within the WST features compared to real speech.

IV. RESULTS AND ANALYSIS

A. Analysis of WST Parameters (RQ1)

Table I summarizes the performance of the proposed front-ends across varying parameter settings. As shown in the top section of the table, the optimal configuration for WST-X1 is $J = 2, Q = 10, M = 2$. We observe the following:

- **Scattering Scale (J):** Performance degrades as J increases (Rows 3-6), suggesting that deepfake artifacts reside in short-term local acoustic variations. Thus, a small J is essential to prevent over-smoothing of these cues.
- **Wavelets Per Octave (Q):** A higher Q consistently boosts performance (Rows 1-3), as high frequency resolution captures the subtle spectral artifacts that distinguish fake speech.
- **Scattering Order (M):** The second order scattering ($M = 2$) outperforms both $M = 1$ and $M = 3$. Although $M = 1$ captures spectral energy envelopes, it lacks the capacity to characterize the modulation dynamics essential for detection. Conversely, the performance drop observed at $M = 3$ suggests that higher-order interactions exhibit diminishing energy, likely contributing to overfitting rather than to the extraction of informative features. We therefore conclude that second-order scattering is sufficient.

As shown in the bottom section of Table I, the optimal configuration for WST-X2 is $J = 2, L = 10, M = 2$. The trends for the scattering scale J and the scattering order M are consistent with those observed for WST-X1. Therefore, we focus on analyzing the impact of the angular resolution parameter L as follows:

- **Angular Resolution (L):** Performance improves as L increases (Rows 1-6 and 7-11) and peaks at $L = 10$. This underscores the critical role of *directional* resolution, as a higher L provides a more granular analysis of the variations of the feature map along different axes, thereby facilitating a more effective localization of forgery artifacts.

B. WST-X Series vs. Mel & Linear & CQ Filterbank (RQ2)

Table II compares the WST-X series with the mel, linear, and constant-Q filterbanks. We observe performance gains from mel to constant-Q, suggesting that mel filters (which emphasize low frequencies to mimic human perception) may mask deepfake artifacts in the higher frequency range. Moreover, WST-X1 and WST-X2 achieve lower minDCF than both the baseline PT-XLSR and the constant-Q filterbank, demonstrating their efficacy in capturing subtle acoustic artifacts.

TABLE II: Comparison of WST-X series feature extractor (FE) with pure DSP (Mel, Linear, and Constant-Q filterbanks) and SSL (PT-XLSR) on Deepfake-Eval-2024. Best results are in **bold**, and second-best are underlined.

FE	minDCF \downarrow	EER (%) \downarrow	F1 (%) \uparrow	AUC (%) \uparrow
WST-X1	0.3408 (± 0.0161)	14.18 (± 0.63)	81.66 (± 0.58)	92.50 (± 0.40)
WST-X2	<u>0.3567</u> (± 0.0081)	<u>14.84</u> (± 0.40)	<u>81.83</u> (± 0.47)	<u>92.43</u> (± 0.23)
Mel	0.9158 (± 0.0074)	41.97 (± 0.51)	14.54 (± 0.84)	62.89 (± 0.59)
Linear	0.7243 (± 0.0138)	31.28 (± 0.41)	50.28 (± 1.26)	<u>75.36</u> (± 0.50)
CQ	0.6356 (± 0.0165)	27.53 (± 0.56)	71.56 (± 0.86)	88.35 (± 0.60)
PT-XLSR	0.4052 (± 0.0124)	20.40 (± 0.54)	77.19 (± 0.65)	90.21 (± 0.41)

C. WST-X Series vs. PT-XLSR (RQ3)

Table II shows that WST-X1 and WST-X2 reduce minDCF by 15.89% and 11.97%, respectively, over the PT-XLSR baseline, confirming that WST's deformation-stable modulation features effectively complement SSL semantic representations, thereby improving deepfake detection performance.

D. Visualization and Interpretability

Fig. 3 compares front-end representations of real speech with deepfakes generated by Qwen2.5-Omni. Visual evidence confirms that conventional features (a-c) often smooth over subtle cues, whereas WST representations (d-e) explicitly reveal fine-grained synthesis artifacts, as marked by the blue bounding boxes. Thus, the WST-X series front-end excels at capturing these subtle artifacts, thereby enhancing the robustness and discriminative capability of SDD systems.

V. CONCLUSIONS

We introduced the WST-X series, a novel family of feature extractors for interpretable speech deepfake detection. We demonstrated that maintaining a small averaging scale with high-frequency and directional resolutions was key to capturing transient spectro-temporal artifacts. These findings suggest that modern synthesis traces are embedded in subtle modulations often overlooked by conventional feature representations. Possible future research directions include exploring the WST's potential in deepfake source tracing tasks.

ACKNOWLEDGMENT

This work was supported by the Finnish AI-DOC project “Explainable Speech Deepfake Characterization” (Decision No. VN/3137/2024-OKM-6), and the Research Council of Finland, project “SPEECHFAKES” (Decision No. 349605). D.C. is supported by PR[AI]RIE-PSAI (France-2030) and worked under the auspices of the Italian National Group of Mathematical Physics (GNFM) of INdAM.

REFERENCES

[1] Kai Zhang et al. Multi-View Collaborative Learning Network for Speech Deepfake Detection. In *Proceedings of the AAAI Conference on Artificial Intelligence*, pages 1075–1083, 2025.

[2] Zhe Ye et al. Amplifying discriminative distortions: A generative latent feature reinforcement framework for audio spoofing detection. *Expert Systems with Applications*, page 130206, 2025.

[3] Yinlin Guo et al. Audio deepfake detection with self-supervised wavlm and multi-fusion attentive classifier. In *ICASSP 2024-2024 IEEE International Conference on Acoustics, Speech and Signal Processing (ICASSP)*, pages 12702–12706. IEEE, 2024.

[4] Xi Xuan et al. Fake-mamba: Real-time speech deepfake detection using bidirectional mamba as self-attention’s alternative. In *Proceedings of the IEEE ASRU*, 2025.

[5] Hoan My Tran et al. Leveraging SSL Speech Features and Mamba for Enhanced DeepFake Detection. In *Interspeech 2025*, pages 5323–5327, 2025.

[6] Hao Gu et al. Allm4add: Unlocking the capabilities of audio large language models for audio deepfake detection. In *Proceedings of the 33rd ACM International Conference on Multimedia*, pages 11736–11745, 2025.

[7] Md Sahidullah et al. A comparison of features for synthetic speech detection. In *Proceedings of Interspeech 2015*, pages 2087–2091, 2015.

[8] Abderrahim Fathan et al. Mel-spectrogram image-based end-to-end audio deepfake detection under channel-mismatched conditions. In *2022 IEEE international conference on multimedia and expo (ICME)*, pages 1–6. IEEE, 2022.

[9] Massimiliano Todisco et al. Constant q cepstral coefficients: A spoofing countermeasure for automatic speaker verification. *Computer Speech & Language*, 45:516–535, 2017.

[10] Arun Babu and others. XLS-R: Self-supervised Cross-lingual Speech Representation Learning at Scale. In *Interspeech 2022*, 2022.

[11] Wei-Ning Hsu et al. Hubert: Self-supervised speech representation learning by masked prediction of hidden units. *IEEE/ACM transactions on audio, speech, and language processing*, 29:3451–3460, 2021.

[12] Vineel Pratap et al. Scaling speech technology to 1,000+ languages. *Journal of Machine Learning Research*, 25(97):1–52, 2024.

[13] International Organization for Standardization. ISO/IEC 30107-3:2023: Information technology – Biometric presentation attack detection – Part 3: Testing and reporting. Technical report, International Organization for Standardization, 2023.

[14] Stéphane Mallat. Group invariant scattering. *Communications on Pure and Applied Mathematics*, 65:1331–1398, 2012.

[15] Joan Bruna et al. Invariant scattering convolution networks. *IEEE transactions on pattern analysis and machine intelligence*, 35(8):1872–1886, 2013.

[16] Georgios Valogiannis et al. Towards an optimal estimation of cosmological parameters with the wavelet scattering transform. *Physical Review D*, 105(10):103534, 2022.

[17] Fatemeh Khatami et al. Origins of scale invariance in vocalization sequences and speech. *PLoS computational biology*, 14(4):e1005996, 2018.

[18] Alessandro Licciardi et al. Whalenet: A novel deep learning architecture for marine mammals vocalizations on watkins marine mammal sound database. *IEEE Access*, 2024.

[19] Zhiyu Li et al. FAST_QR: Fast, accurate and stable quantile regression for time-series analysis via adaptive Huber smoothing. In *2026 IEEE International Conference on Acoustics, Speech and Signal Processing (ICASSP)*. IEEE, 2026.

[20] Nuria Alina Chandra et al. Deepfake-eval-2024: A multi-modal in-the-wild benchmark of deepfakes circulated in 2024, 2025.

[21] Mathieu Andreux et al. Kymatio: Scattering transforms in python. *Journal of Machine Learning Research*, 21(60):1–6, 2020.

[22] Beylkin et al. Fast wavelet transforms and numerical algorithms i. *Communications on pure and applied mathematics*, 44(2):141–183, 1991.

[23] Mallat Stephane. A wavelet tour of signal processing, 1999.

[24] Xin W. Investigating self-supervised front ends for speech spoofing countermeasures. In *The Speaker and Language Recognition Workshop (Odyssey 2022)*, pages 112–119, 2022.

[25] Xi Xuan et al. Multilingual Source Tracing of Speech Deepfakes: A First Benchmark. In *5th Symposium on Security and Privacy in Speech Communication*, pages 27–34, 2025.

[26] Xi Xuan et al. Wavesp-net: Learnable wavelet-domain sparse prompt tuning for speech deepfake detection. In *ICASSP 2026-2026 IEEE International Conference on Acoustics, Speech and Signal Processing (ICASSP)*. IEEE, 2026.

[27] Yuankun Xie et al. Detect all-type deepfake audio: Wavelet prompt tuning for enhanced auditory perception. In *Proceedings of the AAAI Conference on Artificial Intelligence*, 2026.

[28] Héctor Delgado et al. Asvspoof 5 evaluation plan. *Onlyne*. Available: https://www.asvspoof.org/file/ASVspoof5_Evaluation_Plan_Phase2.pdf, 2024.

[29] Bradley Efron et al. Bootstrap methods for standard errors, confidence intervals, and other measures of statistical accuracy. *Statistical science*, pages 54–75, 1986.

[30] Brian McFee et al. librosa: Audio and music signal analysis in python. *SciPy*, 2015:18–24, 2015.

[31] Hideyuki Oiso et al. Prompt Tuning for Audio Deepfake Detection: Computationally Efficient Test-time Domain Adaptation with Limited Target Dataset. In *Interspeech 2024*, pages 2710–2714, 2024.

[32] Juan M. Martín-Doñas et al. Exploring Self-supervised Embeddings and Synthetic Data Augmentation for Robust Audio Deepfake Detection. In *Interspeech 2024*, pages 2085–2089, 2024.